Cement & Concrete Composites 30 (2008) 769–778

Contents lists available at ScienceDirect

Cement & Concrete Composites

journal homepage: www.elsevier.com/locate/cemconcomp

Development of self-leveling screed based on calcium sulfoaluminate cement: Modelling of curling due to drying

J.F. Georgin, J. Ambroise, J. Péra *, J.M. Reynouard

LGCIE, Institut National des Sciences Appliquées de Lyon, Domaine Scientifique de la Doua, Bâtiment J. Tuset, 12, Avenue des Arts, 69 621 Villeurbanne Cedex, France

ARTICLE INFO

Article history:
Received 5 May 2008
Received in revised form 4 June 2008
Accepted 12 June 2008
Available online 20 June 2008

Keywords:
Calcium sulfoaluminate cement
Curling
Hydro-mechanical behavior
Modelling
Moisture diffusion

ABSTRACT

The development of cement-based screed unbound to its support is still limited because of the curling that occurs at the corners and perimeter of the screed. This phenomenon is mainly due to the moisture gradient that appears within the thickness of the screed: the upper surface dries and shrinks, whereas lower regions dry less and stay wetter. This paper demonstrates this phenomenon can be mitigated through the use of calcium sulfoaluminate cement instead of ordinary Portland cement. Experiments utilizing an original, specially designed device, show that curling is 3.5 times lower when calcium sulfoaluminate cement is used compared to ordinary Portland cement. The moisture gradient within the thickness of the screed is also lower.

A model based on simplified poroelasticity theory describes both fluid transfer and hydro-mechanical coupling. The comparison between experimental and calculated results shows that the model gives a good estimation of the kinetics of the mass loss, and that the numerical simulation is an effective tool to predict curling due to drying.

1. Introduction

Some concrete slabs curl upward at their corners and perimeter. This condition is particularly common with slabs-on-grade [1,2]. When this occurs, corners and edges are unsupported and tend to break under load. This phenomenon is especially marked in screeds that are not bound to their support. As the thermal and acoustic insulation regulations become more and more stringent in Europe, this phenomenon is expected to appear more often. The new regulations require use of a layer of insulating material between the support slab and the screed. Therefore, the bond between the support and the screed is broken, and the latter is able to curl more readily.

The curling phenomenon is mainly due to the moisture gradient present within the thickness of the screed, which in turn leads to differential shrinkage between the top and the bottom of a slab or screed. The top surface dries and shrinks, while the bottom stays wet and undergoes a much smaller amount of change in dimensions [3]. The curling of screeds utilizing Portland cement is very common and, therefore, the development and use of these screeds is limited. One solution to limit curling is to use calcium sulfoaluminate cement, as shown in a previous paper [4]. Use of such cement leads to lower drying shrinkage compared with the use of Portland cement.

The present paper is divided into two parts: in the first part, an experimental study is reported, using an original, specially designed, device to compare the behavior of screeds based on:

- Portland cement (OPC).
- Calcium sulfoaluminate cement (CSA).
- Calcium sulfoaluminate + anti-shrinkage agent (CSA + polyol).

In the second part, a model is developed to better understand the physical mechanisms involved within the CSA screed under going desiccation. Theoretical basis for the modelling used to describe both fluid transfer and hydro-mechanical coupling is presented. A simplified poroelasticity approach is used based upon the numerical results obtained by several authors [5–8].

2. Experimental

2.1. Materials and mixture proportions of screeds

The mixture proportions of the screeds were based either on ordinary Portland cement (OPC) or calcium sulfoaluminate cement (CSA) (Table 1).

OPC was a CEM I 52.5 Type according to the European Standard ENV 197-1. Limestone powder was used as supplementary fine material. Its influence on shrinkage at early age has been studied by Bouasker et al. [9]. The system of chemical admixtures in the OPC screed was composed of: a liquid polycarboxylate as

* Corresponding author. Tel.: +33 4 72 43 82 96; fax: +33 4 78 94 98 07.
E-mail address: Jean.Pera@insa-lyon.fr (J. Péra).

0958-9465/$ - see front matter © 2008 Elsevier Ltd. All rights reserved.
doi:10.1016/j.cemconcomp.2008.06.004

Table 1
Mixture proportions of screeds (kg/m^3)

Material	OPC	CSA
OPC CEM I 52.5	300	20
CSA		300
Limestone powder	100	80
Sand (0/5 mm)	1350	1350
Viscosity Modifying Agent (VMA)	0.45	1.25
Superplasticizer (SP)	8	6
Water	320	320

superplasticizer (SP), to get the desired fluidity; and, a viscosity modifying agent (VMA), a modified starch stable in the high-pH basic environment of OPC [10,11].

The CSA cement was composed of 80% CSA clinker and 20% recrystallized gypsum (RG). RG is a by-product of the manufacture of phosphoric acid by the Prayon PH2 process, with two hemi-hydrate stages followed by a di-hydrate process producing co-crystallized gypsum with low P_2O_5 content [12]. The pure gypsum content of RG determined by DTA-TGA was 89.4%. The composition of CSA clinker was as follows:

- $Ca_4Al_6O_{12}SO_4$ (yeelimite): 75.5%
- β-Ca_2SiO_4 (belite): 11.1%
- $Ca_3Fe_2TiO_9$ (perovskite): 9.2%
- $Ca_{12}Al_{14}O_{33}$ (mayenite): 2.6%

OPC was added to the recipe of the CSA screed in order to get shrinkage compensation, by forming swelling ettringite from the reaction of CSA, OPC, and water. The system of chemical admixtures was composed of:

- A superplasticizer (polycarboxylate) to get the desired fluidity for three hours, which is required for on site-applications.
- An anti-shrinkage agent: a polyether polyol. The influence of polyol on the drying and curling of self-leveling screeds based on calcium sulfoaluminate cement was described in a previous paper [13]. When polyol was added to the mixture (0.63% of the cementitious material content), curling was reduced by 23%. Polyol also reduced drying shrinkage by 40%, but did not affect the mass loss of the screed and the porous distribution.
- A viscosity modifying agent (polyvinyl alcohol + Welan gum) to avoid sedimentation and bleeding.

The quantities of SP and VMA were adjusted to keep the water content constant in both types of screeds at 320 L/m^3.

The fluidity of the mortar was measured by means of the static spread of a truncated cone having the following dimensions: $\varnothing_{inf}$ = 95 mm; $\varnothing_{sup}$ = 55 mm; h = 70 mm. Mortar was considered as self-leveling when the spread reached 250–270 mm.

2.2. Measurement of the curling of screeds

A special measuring device was developed to simulate the curling phenomenon, which is shown in Figs. 1–3 [14] and composed of the following:

- A mold, in which a mortar slab with dimensions 330 × 330 × 30 mm can be cast. The sides of the mold had 1° relief angle in order to permit the vertical displacement of slab corners and the perimeter. All the faces of the mold are treated (teflon coating deposited at high temperature) in order to prevent bond between the mold and the mortar. The thickness of the mold is very close to that typically used at a construction site in France, 40–50 mm.

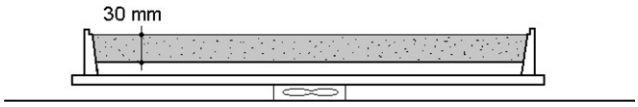

Fig. 1. Cross-section of the equipment showing the sample on the balance.

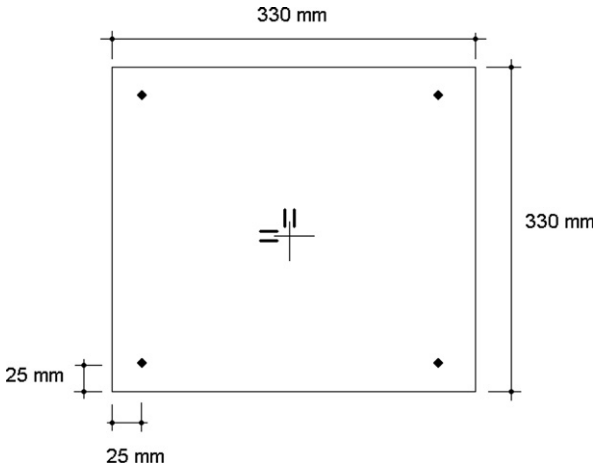

Fig. 2. Top view of the equipment showing the position of the LVDT sensors: two for horizontal shrinkage measurement and four for vertical displacement of corners.

- A balance to continuously measure the mass loss of the whole system.

Twenty-four hours after casting the screed, the slab was equipped with four vertical LVDT sensors placed in the corners measuring the vertical displacement; and two horizontal LVDTs measuring the shrinkage occurring at the centre of the slab (Fig. 3). The LVDT's precision was 0.5%. The mold and measuring equipment was stored at 20 °C and 50% RH after casting the screed. Data were recorded automatically each hour after casting. During the first 24 h, the curing regime was maintained at 20 °C and 50% RH.

The mass loss (water-mass) of screeds is shown in Fig. 3. At 28 days, the mass loss of the CSA screed (with and without polyol) was about 20% lower than that of the OPC screed. This can be explained by the higher consumption of mixing water necessary to produce ettringite:

$$4CaO \cdot 3Al_2O_3 \cdot SO_3 + 8[CaSO_4 \cdot 2H_2O] + 6[Ca(OH)_2 + 74H_2O \Rightarrow 3[3CaO \cdot Al_2O_3 \cdot 3CaSO_4 \cdot 32H_2O]. \quad (A)$$

This reaction may explain the lower value of drying shrinkage observed in the CSA screed (Fig. 4). At 20 days, the OPC screed developed shrinkage of 890 μm/m. At the same age, the shrinkage of CSA was only 545 μm/m, or 39% less. The presence of polyol had additional beneficial effect on the shrinkage of CSA screed: the maximum value recorded was only 435 μm/m. Polyol reduced CSA screed shrinkage by 20%, which is less than the value reported in a previous study for a different mixture proportion of the mortar [14].

The curling of screeds is shown in Fig. 5. All the results were obtained when curing the screeds at 20 °C and 50% RH, after having sprayed a curing compound on the top surface of the screed. In Fig. 5, the time scale begins with the time of casting the screed. OPC screed started to curl after 4 days of hydration while CSA-based screeds started to curl after two days of hydration. After 20 days of hydration at 20 °C and 50% RH, the curling of the CSA screed was 3.5 times lower than that of the OPC screed. The curling of (CSA + polyol) screed was nearly seven times lower than that of

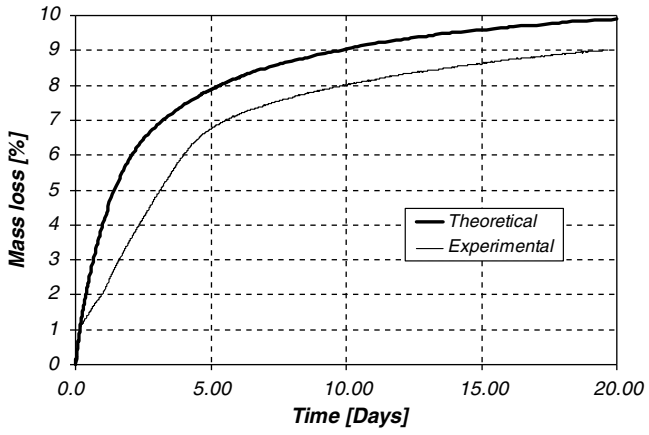

(a) OPC

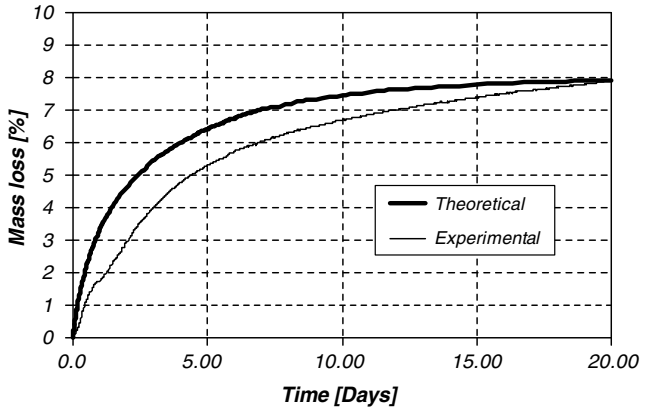

(b) CSA

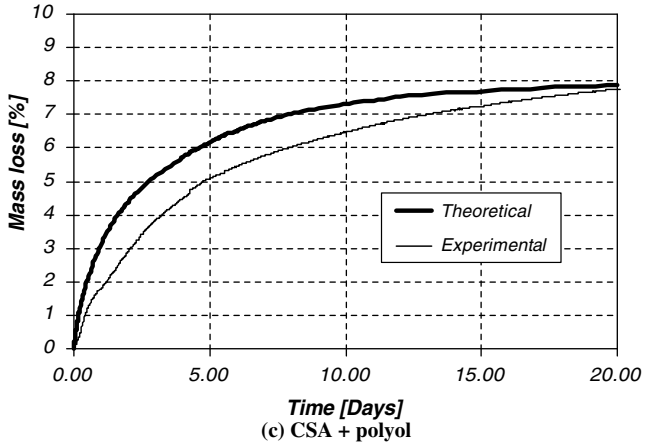

(c) CSA + polyol

Fig. 3. Mass loss of screeds.

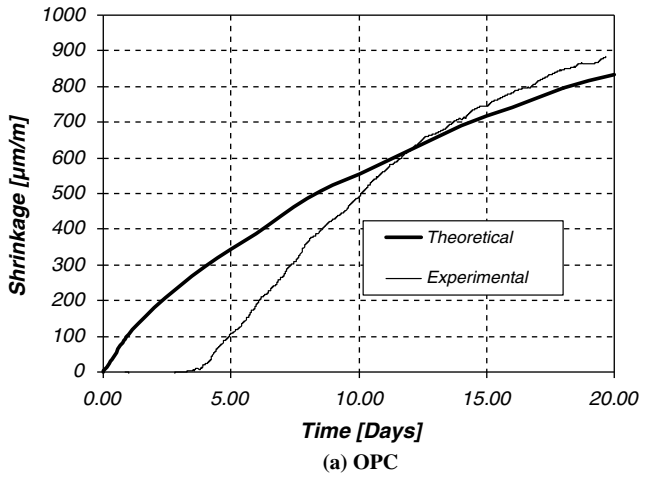

(a) OPC

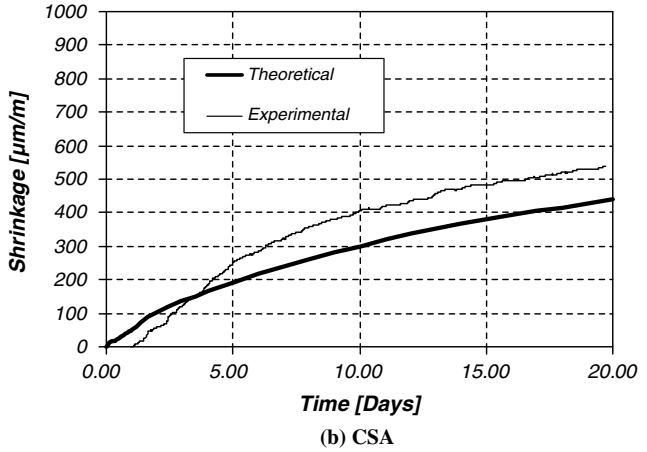

(b) CSA

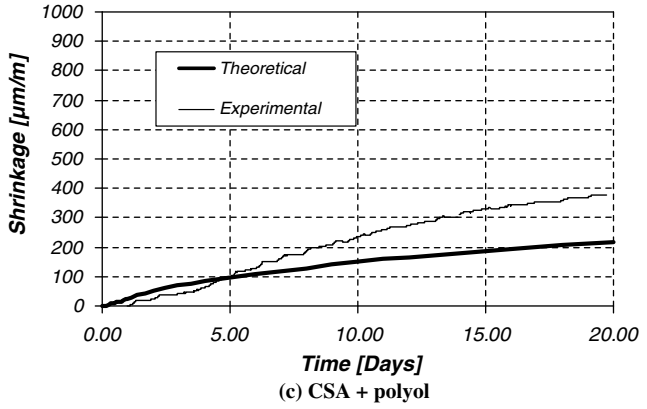

(c) CSA + polyol

Fig. 4. Drying shrinkage of screeds.

the OPC screed. This result is believed to be mainly due to a smaller gradient in the distribution of internal relative humidity within the thickness of the CSA screed compared to OPC screed. The internal relative humidity (RH) was measured by means of two sensors encased in Gore-Tex sleeves placed at 5 mm from the top and the bottom of the screed. The accuracy of the sensors was reported by the manufacturer to be ±0.5% between 10% and 95% RH. The Gore-Tex allowed vapor transmission while preventing the penetration of liquid moisture and ions that could invoke erroneous measurements. The RH measurements are reported in Fig. 6. The RH gradient was always about 13–15% in the CSA screeds, while it ranged from 19% to 37% in the OPC screed. Furthermore, it was observed that the CSA screed dried more homogeneously than the OPC screed (see Fig. 6).

3. Modelling

3.1. Modelling of isothermal drying

The theoretical modelling of drying shrinkage in non-saturated porous media presented in this paper is based on the theory of poroelasticity proposed by Coussy [6]. The two basic concepts of Coussy's theory are:

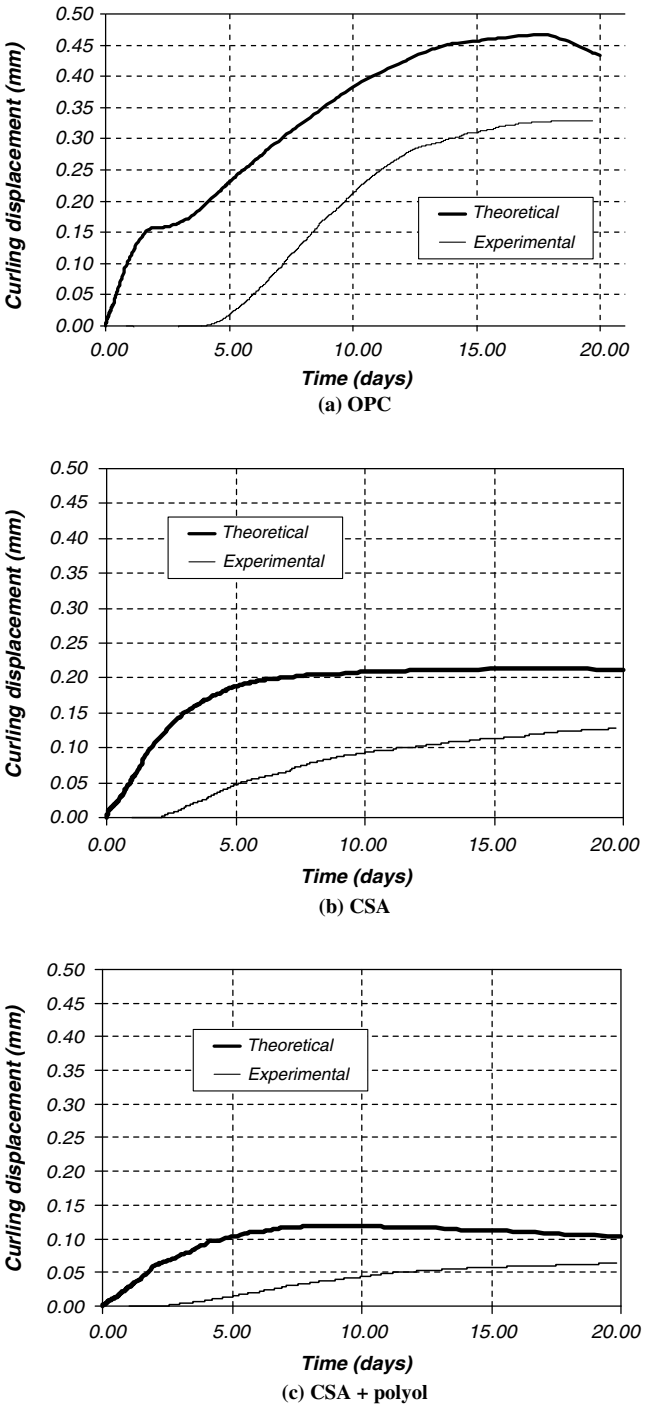

Fig. 5. Curling of screeds.

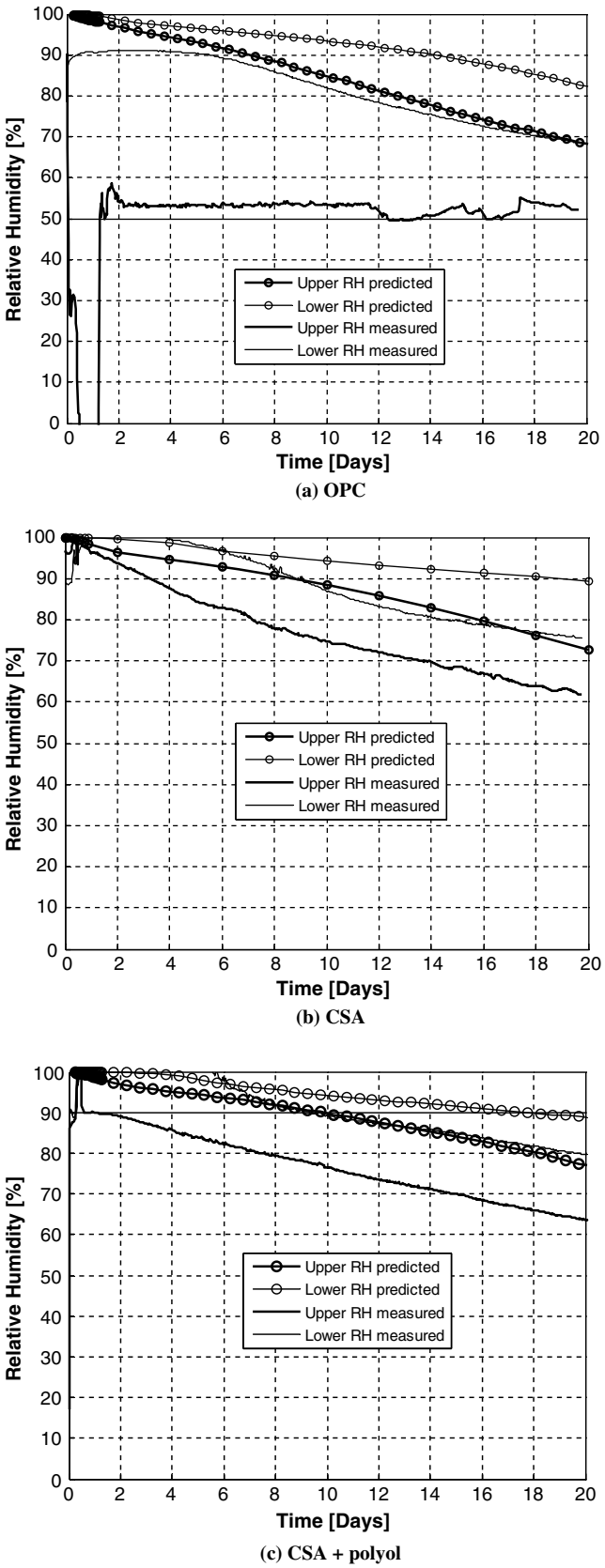

Fig. 6. Distribution of internal humidity within the thickness of the screeds.

- At the macroscopic level, a cement-based porous material Ω can be viewed as the superposition of $(n + 1)$ mechanically interacting media; n represent the n saturating fluids, while the remainder corresponds to the deformable skeleton. An elementary system $d\Omega$ extracted from Ω is constituted of a connected porous space through which fluid mass exchanges occur and a solid matrix that possibly includes an occluded porosity through which no filtration occurs. The n saturating fluid phases are the water in liquid form (index l), its vapor (index v), and the dry air (index a), with the two latter phases forming a mixture. Index i is used to design an unspecified fluid phase: i = l, v, or a.

- Owing to the relative motion of the saturating fluids with respect to the skeleton, the elementary system $d\Omega$ did not have

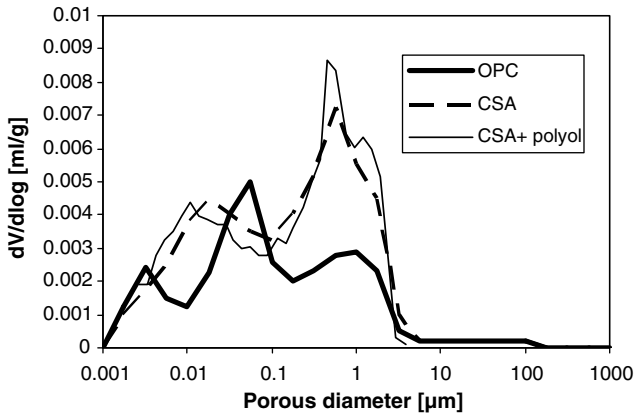

Fig. 7. Experimental pore-size distribution.

the same fluid mass after deformation as it had before. In this sense, it is an open system exchanging fluid mass with the outside.

The principle of mass conservation leads to:

$$\frac{dm_l}{dt} + \mathrm{div}(W_l) + m_{l\to v} = 0, \quad (1)$$

$$\frac{dm_v}{dt} + \mathrm{div}(W_v) + m_{v\to l} = 0, \quad (2)$$

$$\frac{dm_a}{dt} + \mathrm{div}(W_a) = 0, \quad (3)$$

where w_i is the relative flow vector of fluid mass associated with phase i (i = l, v or a), and $(m_{l\to v}dt\,d\Omega)$ represents the liquid mass changing into vapor in the elementary system $d\Omega$ during the time interval dt with:

$$m_{l\to v} = -m_{v\to l}. \quad (4)$$

Terms m_i are linked to the total porosity, φ the water saturation S_l, and the mass density ρ_i of phase i, according to:

$$m_l = \phi\rho_l S_l, \quad (5)$$

$$m_v = \phi\rho_v(1 - S_l), \quad (6)$$

$$m_a = \phi\rho_a(1 - S_l). \quad (7)$$

Assuming the decoupling of all transport mechanisms, the movement of the liquid phase is governed by the Darcy's law, giving the velocity of the liquid phase:

$$w_l = -\rho_l \frac{k}{\eta_l} k_{rl}(S_l)\mathrm{grad}(p_l), \quad (8)$$

where η_l is the dynamic viscosity of the liquid, k is the permeability of the porous material, k_{rl} is the relative permeability associated with the liquid phase, and p_l is the liquid pressure.Considering the mass conservation of the liquid phase plus the vapor phase, the following equation is obtained:

$$\frac{d(\phi\rho_l S_l + \phi\rho_v(1 - S_i))}{dt} + \mathrm{div}(w_l + w_v) = 0, \quad (9)$$

where w_v is the velocity of the vapor phase.Numerical studies [15,5] have shown that it was possible to neglect vapor transport under its convective form as well as the term $\varphi\ \rho_v(1 - S_l)$. Therefore, Eq. (9) becomes:

$$\frac{d(S_l)}{dt} + \mathrm{div}\left(\frac{k}{\phi\eta_l} k_{rl}(S_l)\mathrm{grad}(p_l)\right) = 0. \quad (10)$$

Instead of knowing the liquid pressure versus water saturation, chemical potential balance at liquid and vapor interface allows to obtain further information. Indeed, the capillary curve gives the capillary pressure value versus the water saturation as:

$$P_c = p_c(S_l). \quad (11)$$

Thus, neglecting the variation of gas pressure compared to liquid pressure, as the capillary pressure is equal to:

$$P_c = p_g - p_l. \quad (12)$$

Eq. (10) becomes:

$$\frac{d(S_l)}{dt} + \mathrm{div}(D(S_l)\mathrm{grad}(S_l)) = 0. \quad (13)$$

$D(S_l)$ is the transport coefficient given by:

$$D(S_l) = -\frac{k}{\phi\eta_l} k_{rl}(S_l)\frac{dp_c}{dS_l}. \quad (14)$$

The relative water permeability could be described by the Mualem's model:

$$K_{rl}(S_l) = \sqrt{S_l}\left[1 - (1 - S_l^{\frac{1}{m}})^m\right]^2, \quad (15)$$

where m is a parameter given in the literature [16].

3.2. Drying shrinkage

Coussy et al. [7] presented the new concept of equivalent pore pressure, π, in which the average pressure, p^*, depends on the pressure of all phases present in the porous space and the sum, U, of the energy of all interfaces (liquid–gas, liquid–solid and gas–solid). The equivalent pore pressure is given by:

$$\pi = p^* - U. \quad (16)$$

With

$$P^* = S_l p_l + S_g p_g = p_g - S_l P_c. \quad (17)$$

And

$$U = \int_{S_l}^{1} p_c(S_l)dS_l. \quad (18)$$

In standard unsaturated poroelasticity [6], the volumetric strain, ε, is linked to the volumetric mean stress, σ, and to the fluid equivalent pore pressure, π, through:

$$\varepsilon = \frac{\sigma + b\pi}{K_0}, \quad (19)$$

K_0 is the bulk modulus of the skeleton, i.e. the associated "dry" material, while b is the Biot coefficient expressed in the following form [6]:

$$b = 1 - \frac{K_0}{K_S}. \quad (20)$$

K_0 is a function of the Young modulus E and the Poisson's ratio v:

$$K_0 = \frac{E}{3(1 - 2v)}. \quad (21)$$

K_s is the bulk modulus of the matrix, i.e. the solid part of the skeleton. Assuming free deformations, i.e. geometrical variation without structural effect or restrained boundaries ($\sigma = 0$), infinitesimal shrinkage deformation is evaluated from Eq. (19) to give:

$$d\varepsilon = \frac{b}{K_0} d\pi. \quad (22)$$

From Eqs. (16)–(18), Eq. (23) is obtained.

$$d\pi = dp^* - dU = dp_g - S_l dp_c. \quad (23)$$

Assuming that the gas pressure variation is very weak, this leads to:

$$d\varepsilon = -\frac{bS_l}{K_0} dp_c. \quad (24)$$

The knowledge of the function written in Eq. (12) under its inverse form $S_l(p_c)$, modifies the latter equation to:

$$\varepsilon(S_l) - \varepsilon(l) = \int_l^{S_l} d\varepsilon = \int_{S_l}^{l} \frac{bS_l}{K_0} dp_c. \quad (25)$$

3.3. Numerical simulations

3.3.1. Identification of the parameters linked to the material

In this section, numerical results, obtained by the above-developed approach, are compared to the experimental results obtained from CSA and OPC screeds. The aim of this modelling is not to fit modelling parameters in order to give a good estimation of the measurements obtained in the curling test, but to point out adequate procedures allowing the identification of these parameters. This is why preliminary experiments were carried out in order to identify the transfer behavior of both CSA and OPC screeds, and characterize their hydro-mechanical coupling. A good knowledge of the behavior of a porous material is generally provided from experimental water desorption and adsorption isotherms, which correspond to the measurement of mass water content at equilibrium versus relative humidity environment. Moreover, assuming that the internal gaseous mixture is at the atmospheric pressure, the liquid–vapor equilibrium is ruled by Kelvin's law which is expressed in the form:

$$P_c = -\frac{\rho_l RT}{M_v} \ln h, \quad (26)$$

where R is the constant of ideal gas, M_v the vapor molar mass, T the absolute temperature, h the relative humidity, ρ_l the liquid mass density, and p_c the macroscopic capillary pressure.

Several desorption experiments were carried out for three different relative humidities: 90%, 70%, and 50%. From the kinetics of desorption, it was possible to identify the degree of saturation at equilibrium which is useful to plot the desorption curve, also called the capillary curve.

In this work, a modelling approach was proposed to determine in a different way both CSA and OPC isotherms. Previous experimental results were used and compared to results obtained by this new method in order to check its consistency. The idea of this approach was to construct the isotherm curve from the pore-size distribution curve (Fig. 7). The pore-size distribution curves for both CSA and OPC screeds were obtained from a mercury porosimetry intrusion analysis (Fig. 8). In a non-saturated material, the porous radius r that is concerned by the capillary pressure defines the boundary between liquid and gas phases. In other words, all porous medium where radius is smaller than r is saturated and all porous medium where radius is higher than r is filled by gas (see Fig. 9). As a consequence, the degree of saturation S_l can be estimated from the following equation:

$$S_l(r) = \frac{V_{water} + V_{adsorbed}}{V_{totsl}}, \quad (27)$$

where V_{water} and V_{total} are determined from the cumulative pore-size distribution curve as illustrated in Fig. 8 for the (OPC) case.

The adsorbed water $V_{adsorbed}$ is estimated by assuming that the pores have a cylindrical shape:

$$V_{adsorbed} = \int_{R_p}^{\infty} [\pi r^2 - \pi(r-\delta)^2] dt, \quad (28)$$

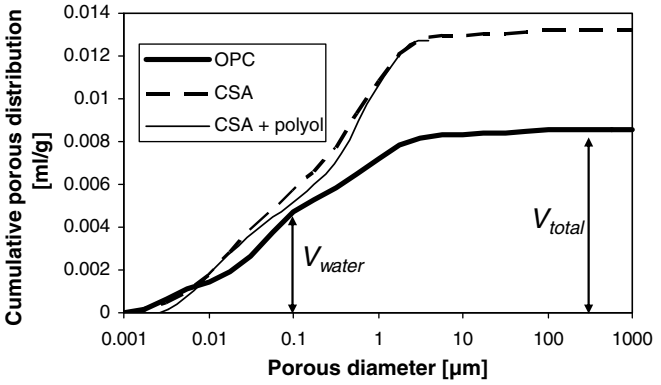

Fig. 8. Cumulative pore-size distribution.

where r is the radius of the cylindrical pore and l is the length of this pore. The adsorbed water layer δ is linked to the relative humidity h by the relationship proposed by Bentz [17]:

$$\delta(h) = 0.395 - 0.189 \ln[-\ln(h)]. \quad (29)$$

Additionally, the corresponding capillary pressure is calculated by the Washburn equation:

$$P_c = \frac{2\gamma}{r} \cos(\theta), \quad (30)$$

where γ is the water surface tension ($0.0728\ Nm^{-1}$), θ the water contact angle (0°), r the radius of the capillary.

From Eqs. (27)–(29), the theoretical capillary curves $p_c(S_l)$ relative to CSA, CSA + polyol, and OPC screeds can be obtained. These curves are plotted in Fig. 10. Kelvin's equation (26) leads to the theoretical desorption curves shown in Fig. 11. Desorption measurements carried out on CSA, CSA + polyol, and CPA screeds are compared to the capillary curves estimated from the cumulated porous distribution. It can be observed that experimental results are close to the theoretical curves.

The hydro-mechanical behavior is described by Eq. (25), in which appears the Biot coefficient b. In order to identify its value, drying shrinkage was measured on prismatic specimens (40 mm × 40 mm × 160 mm). All boundary faces were subjected to 50% relative humidity. Assuming to be under free deformation or unrestrained configuration ($\sigma = 0$), Eq. (25) becomes:

$$\varepsilon(S_l = 0.5) = \frac{b}{K_0} \int_{0.5}^{1} S_l(p_c) dp_c. \quad (31)$$

The functions drawn in Fig. 12 were derived by inversion of those presented in Fig. 10. The free shrinkage prediction was estimated by Eq. (31), giving the fitted parameter b for each type of mortar (Table 2).

3.3.2. Curling test simulation

Taking into account the characteristics of the CSA material previously estimated, hydro-mechanical simulation of the curling experiment was performed in 3D configuration. A quarter of the screed was modeled as shown in Fig. 13. Lateral sides S1, S2 and the top surface S6 were supposed to be free in displacement, while symmetric configuration led horizontal displacements of lateral sides S3 and S4 to be restrained. The bottom surface of the screed S5 was placed on simple support in order to allow only vertical displacements. Only the top of the screed was exposed to 50% relative humidity. More precisely, a convective boundary was used to describe the exchange of humidity between the exposed surface and the surrounding atmosphere. This condition is expressed as follows:

$$w = \beta(S_l - S_l^{limit}), \quad (32)$$

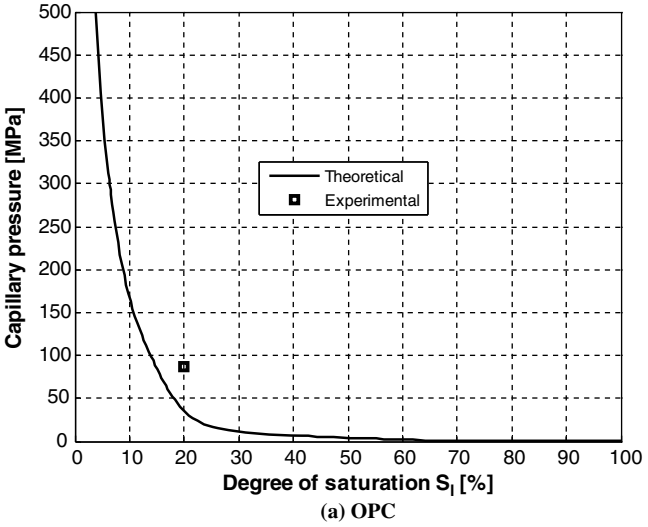

(a) OPC

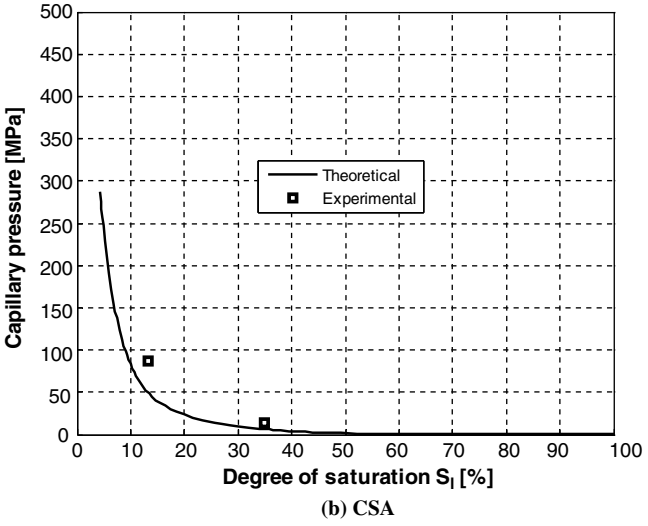

(b) CSA

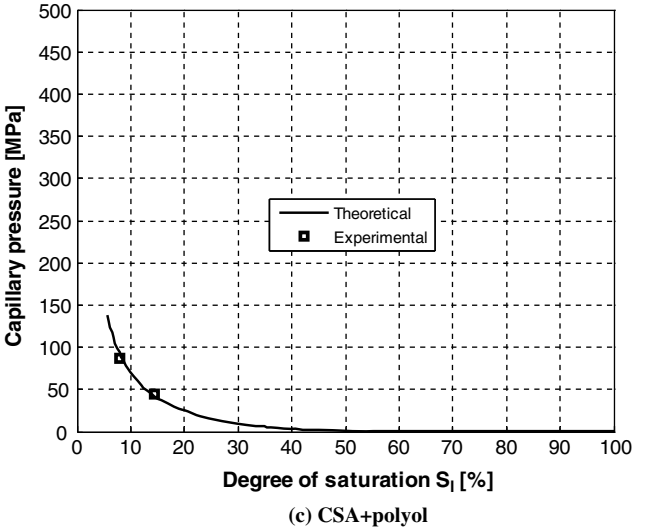

(c) CSA+polyol

Fig. 9. Theoretical capillary curves $P_c(S_l)$.

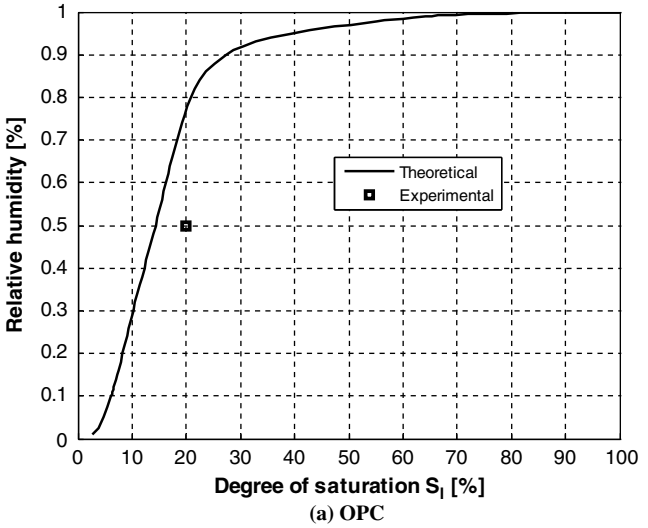

(a) OPC

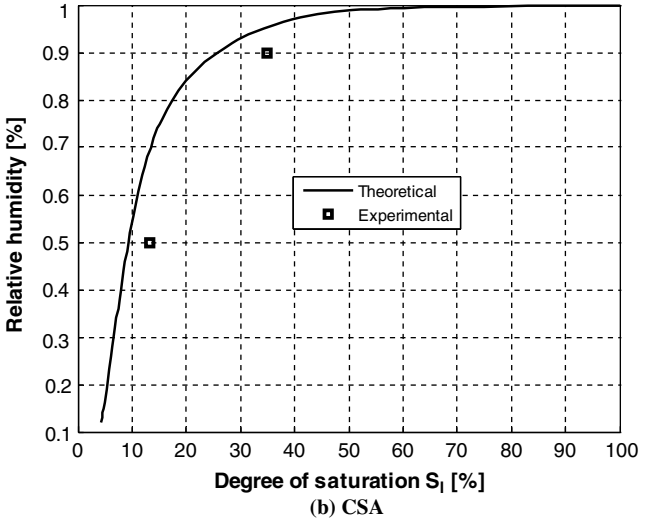

(b) CSA

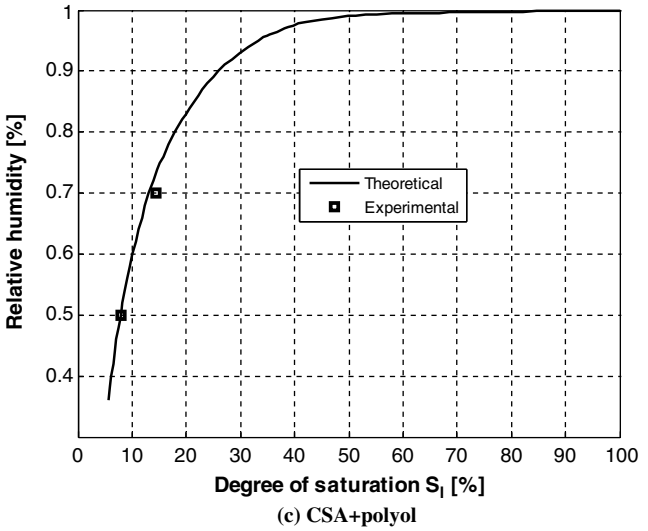

(c) CSA+polyol

Fig. 10. Desorption curves.

where w is the moisture flux normal to the exposed surface, β the hydral convection coefficient ($\beta = 7.5 \times 10^{-5}$ mm s^{-1}), S_l the degree of saturation inside the screed, and S_l^{limit} is the degree of saturation in the superficial layer of the screed.

A zero flow was imposed on all other sides. Near the drying surface, the mesh was refined in order to better capture the gradient of saturation degree. Finite elements were eight node-prisms, as well as for mechanical resolution, for hydric calculation.

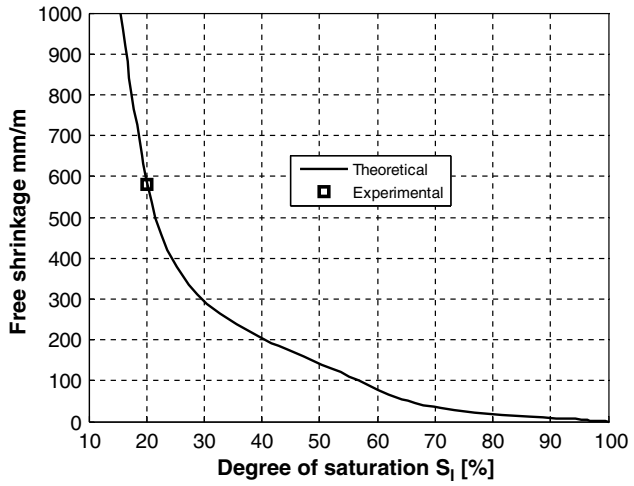

(a) OPC

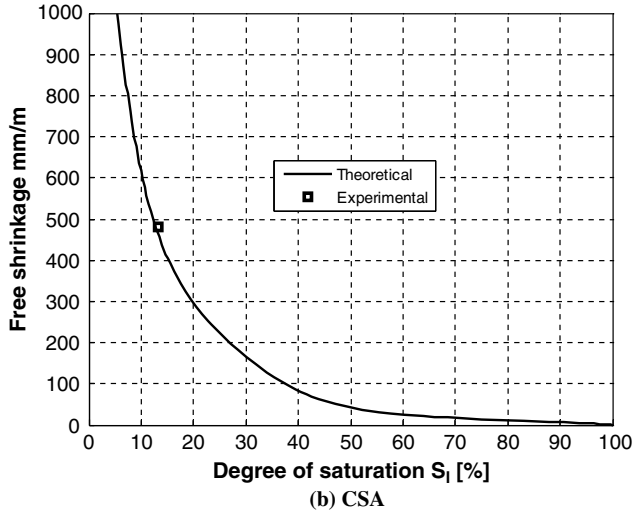

(b) CSA

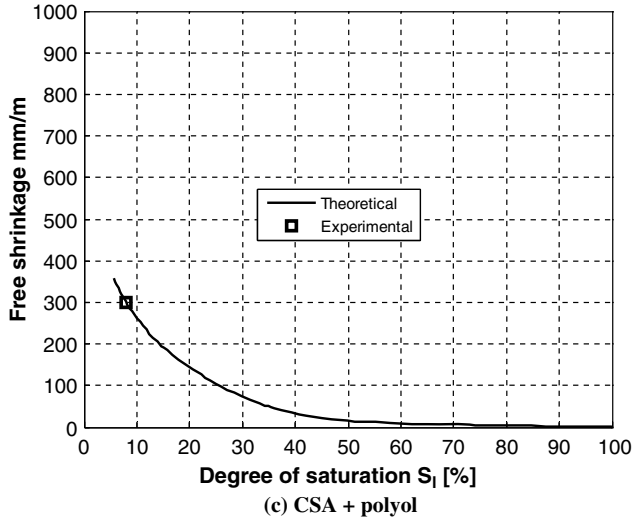

(c) CSA + polyol

Fig. 11. Fitting Biot coefficient.

Simulation of the behavior of the screed started at the end of casting it. Both mechanical and hydric properties changed with increasing time. During the first hours, the constitutive material was completely liquid and the drying process was activated, but the lack of rigidity prevented the screed from curling. The screed exhibited some mechanical stiffness only after several hours of hydration. The evolution of Young modulus and Poisson's coefficient which are linked to the kinetics of hydration was not the focus of this work. Numerical calculation was performed within two steps. Experimentally, the set of the CSA screed occurred after six hours. Therefore, the calculation of the transfer of water from the beginning, i.e. the end of casting the screed, was considered. On the other hand, the mechanical determination started after six hours, when a gradient in the degree of saturation appeared. Experimentally, the mass loss and the internal relative humidity were measured from the beginning, while the device measuring displacements at the corners and the deformation at the middle of the top surface of the screed started after one day. The mass loss of the screed was calculated by integrating the degree of saturation over the screed with the following equation:

$$\Delta m_l = m_l(t) - m_l(t=0). \tag{33}$$

With

$$m_l = \int_v \phi \rho_l S_l \, dV. \tag{34}$$

From mercury porosimetry intrusion analysis, the total porosity was 25% for CSA mortar and 17% for OPC mortar. A last modelling parameter, which was not determined from preliminary experiments, was the permeability k in Eq. (14). Its observed value ($k = 2 \times 10^{-18}\ m^{-2}$) was fitted by considering the initial slope of the mass loss curve of the OPC material.

The comparisons between the experimental and computed values of the mass loss of the screed are shown in Fig. 3. The numerical mass loss results seem to be in poor agreement with the experimental drying kinetics. In the case of OPC screed, modelling prediction overestimated the ultimate experimental mass loss measurement. This difference can be explained by the bleeding which was observed just after casting OPC screed. This water, located on the upper surface of the screed, which rapidly evaporated, led to the decrease of the effective w/c ratio of the OPC mixture. Quantitatively, the difference between numerical and experimental results was about 5%. In the case of CSA screed, the difference observed between ultimate modelling prediction and experimental results was lower. In this approach, water used for hydration was not introduced in the mass balance Eq. (13) as source term. This point can explain the differences observed in the mass loss kinetics in the first few hours after casting for all mixtures.

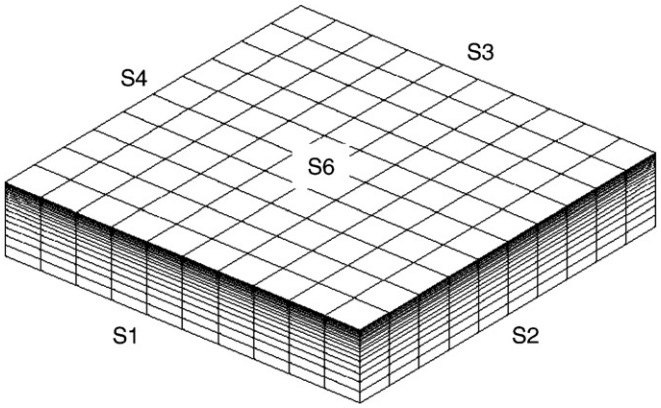

Fig. 12. Finite element mesh for the screed.

Table 2
Fitting values of Biot coefficient on 40 × 40 × 160 mm samples under desiccation

	OPC	CSA	CSA + polyol
Biot coefficient b	0.38	0.3	0.16

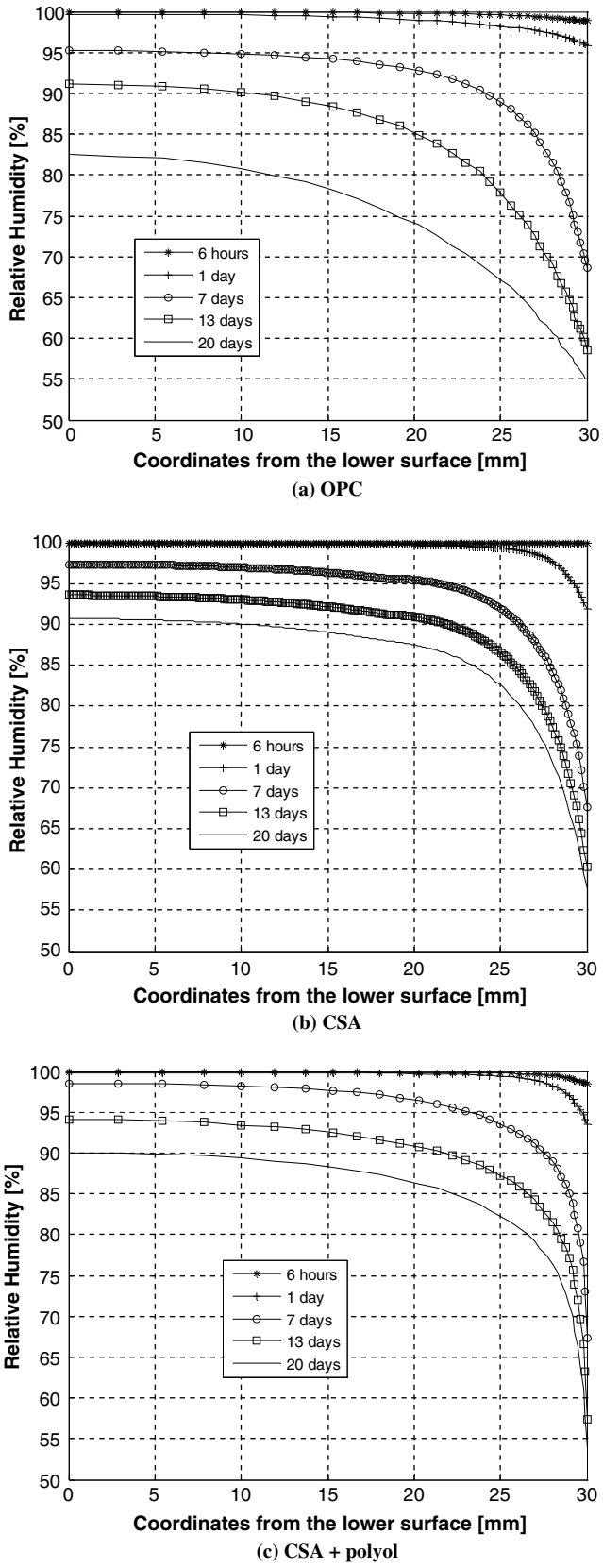

Fig. 13. Gradients of internal relative humidity given by the model.

The evolution of the curling displacement obtained by calculation is compared to the average value of the displacements measured at the four corners of the screed (Fig. 5). Even if simulation started six hours after casting, to be consistent with the experiment, displacements were plotted considering one day as the origin of the time axis. It should be pointed out that both the kinetics of the displacement and the maximum value of the displacement were overestimated by the simplified poroelastic approach. As stated before, the porous distribution and the desiccation test on prismatic sample ($40 \times 40 \times 160$ mm) were used to predict the different responses of each type of screed.

Further analysis of the comparison of shrinkage measurements (Fig. 4) carried out on the upper surface of the screed shows accurate prediction of this modelling approach. Two aspects are important to understand in order to describe the hydro-mechanical behavior of cementitious materials. The first one concerns hydric transport properties, which are essentially given by the porous distribution, and the second one is the coupling level between solid and fluid phases specified by Biot coefficient.

Humidity sensors inside the screed allowed to compare the saturation gradient predicted by the modelling with each value of the measured internal relative humidity. Fig. 13 shows relative humidity gradients given by the calculation at several ages. The measured relative humidity kinetics is compared to numerical results for each mixture in Fig. 6. The comparison of the results shows that prediction is not relevant. But the modelling approach is simplistic and hides other mechanisms such as the material non-homogeneity, the influence of the cement hydration, and the mass transport contribution of gas. Otherwise, humidity sensors locally disturb the humidity gradient and, therefore, also the measurement. Nevertheless, qualitatively, the model confirms that the smaller gradient in the case of CSA screed is responsible of smaller curling.

4. Conclusions

In this work, both experimental and numerical tools were developed in order to improve the knowledge of mechanisms involved in the curling of screeds based on calcium sulfoaluminate cement. From a modelling point of view, a procedure based on simple tests (desiccation test, free shrinkage, and porosity measurement) characterized some important model parameters: the capillary curve and Biot coefficient. In spite of the complexity of assessing all the mechanisms involved during the first few days after casting, the simplified porosity theory is a valid approach to describe the curling phenomenon. Also, it is in good agreement with experimental results. From this analysis, the determination of the porous distribution appears to be crucial to reduce drying shrinkage. The area under the capillary curve obtained from the previous one gives an idea of the level of the interfacial energy acting in the multi-phase material. It is also responsible for the matrix shrinkage. The use of both calcium sulfoaluminate cement and polyol led to a decrease in the area under the capillary curve, leading to observed lower shrinkage values.

Some complementary work is needed to finalize the results obtained from this project. Free shrinkage tests must be carried out under other relative humidity than 50%, in order to confirm the evaluation of Biot coefficient. Finally, the hydration kinetics of cement must be taken into account in order to enhance the capacity of this approach to model hydrating materials.

References

[1] ACI Manual of Concrete Practice 1991 – Part 2. Construction practices and inspection pavements, guide for concrete floor and slab construction. Detroit: ACI 302.1; 1991. p. 40–1.
[2] Walker WW, Holland JA. Design, materials, and construction considerations for reducing the effects of concrete floor curling (warping) and shrinkage. In: Seidler P, editor. Proceedings international colloquium industrial floors '99. Esslingen: Technische Akademie Esslingen), vol. I; 1999. p. 171–80.

[3] Paciorek C. Experimental analysis of the behaviour of structural elements of concrete reinforced by steel fibers. PhD thesis. Béthune, Université d'Artois; 1996. [in French].
[4] Péra J, Ambroise J. New applications of calcium sulfoaluminate cement. Cement Concrete Res 2004;34(4):671–6.
[5] Baroghel-Bouny V, Mainguy M, Lassabatere T, Coussy O. Characterization and identification of equilibrium and transfer moisture properties for ordinary and high-performance cementitious materials. Cement Concrete Res 1999;29:1225–38.
[6] Coussy O. Mechanics of porous continua. New York: John Wiley & Sons; 1995.
[7] Coussy O, Dangla P, Lassabatere T, Baroghel-Bouny V. The equivalent pore pressure and the swelling and shrinkage of cement-based materials. Mater Struct 2004;37(265):15–20.
[8] Coussy O, Eymard R, Lassabatere T. Constitutive modelling of unsaturated drying deformable materials. J Eng Mech ASCE 1998;124(6):658–67.
[9] Bouasker M, Mounanga P, Turcry P, Loukili A, Khelidj A. Chemical shrinkage of cement pastes and mortars at very early age: effect of limestone filler and granular inclusions. Cement Concrete Comp 2008;30(1):13–22.
[10] Rols S, Ambroise J, Péra J. Effects of different viscosity agents on the properties of self-levelling concrete. Cement Concrete Res 1999;29(2):261–6.
[11] Ambroise J, Chabannet M, Rols S, Péra J. Basic properties and effects of starch on self-levelling concrete. In: Cabrera JG, Rivera-Villareal R, editors. Proceedings international RILEM conference on the role of admixtures in high performance concrete. Monterrey: RILEM Publications, 1999. p. 377–86.
[12] Official site of Prayon technologies. <http://www.prayon.com/uk/techn/page_fabr.cfm> [accessed 21.12.07].
[13] Ambroise J, Georgin JF, Péra J. Influence of polyol on the drying and curling of self-leveling screeds based on calcium sulfoaluminate cement. In: Malhotra VM, editor. In: Proceedings 7th CANMET/ACI international conference on durability of concrete. Montreal: ACI SP 234-27; 2006. p. 445–56.
[14] Ambroise J, Georgin JF, Pera J, Reynouard JM. Curling of cement-based screeds. Concrete Sci Eng 2002;4(6):114–20.
[15] Mainguy M. Modèles de diffusion non-linéaires en milieux poreux. Applications à la dissolution et au séchage des matériaux cimentaires. PhD thesis. Paris, Ecole Nationale des Ponts et Chaussées; 1999. [in French].
[16] Mainguy M, Coussy O, Baroghel-Bouny V. The role of air pressure in the drying of weakly permeable materials. J Eng Mech ASCE 2001;127(6):582–92.
[17] Bentz DP, Garboczi EJ, Quenard DA. Modelling drying shrinkage in reconstructed porous materials: application to porous Vycor glass modelling simulation. Mater Sci Eng 1998;6:211–36.